DIRECT NUMERICAL SIMULATION AND THEORIES OF WALL TURBULENCE WITH A RANGE OF PRESSURE GRADIENTS

G.N. Coleman[1], *A. Garbaruk*[2] *and P.R. Spalart*[3]

[1] *Computational AeroSciences, NASA Langley Research Center, Hampton, VA 23681, USA*
[2] *St.-Petersburg State Polytechnic University, St.-Petersburg 195251, Russia*
[3] *Boeing Commercial Airplanes, P.O. Box 3707, Seattle, WA 98124, USA*

gary.n.coleman@nasa.gov

A new Direct Numerical Simulation (DNS) of Couette-Poiseuille flow at a higher Reynolds number is presented and compared with DNS of other wall-bounded flows. It is analyzed in terms of testing semi-theoretical proposals for universal behavior of the velocity, mixing length, or eddy viscosity in pressure gradients, and in terms of assessing the accuracy of two turbulence models. These models are used in two modes, the traditional one with only a dependence on the wall-normal coordinate y, and a newer one in which a lateral dependence on z is added. For pure Couette flow and the Couette-Poiseuille case considered here, this z-dependence allows some models to generate steady streamwise vortices, which generally improves the agreement with DNS and experiment. On the other hand, it complicates the comparison between DNS and models.

1 Introduction

The present study extends that of Johnstone, Coleman and Spalart in 2010, in which a single case of Couette-Poiseuille flow at a relatively low Reynolds number was presented. The purpose was to extend DNS conducted between two parallel plane walls to flows with a range of pressure gradients, relative to the common case of Poiseuille flow which has only a weak favorable gradient, without facing the difficulties of a spatially developing boundary layer. Compared with Poiseuille flow, Couette-Poiseuille requires very little extra coding, but raises severe issues of domain size because of the global vortices. The earlier study appeared to provide a fairly clear if surprising answer to the seemingly simple question of how the law or laws of the wall extend(s) to flows in pressure gradients. The question was couched as follows.

Assuming a constant-stress 'Couette-flow' region in wall-bounded turbulence leads to at least three classical relationships between the derivative of the mean velocity $\mathrm{d}U/\mathrm{d}y$ and the shear stress $-\overline{u'v'}$, the two quantities at the core of turbulence modeling. Expressed in terms of length scales to allow direct comparisons, these include the one leading to the logarithmic law of the wall for the velocity,

$$\frac{u_\tau}{\mathrm{d}U/\mathrm{d}y} = \kappa y_w, \tag{1}$$

where κ is the Kármán constant, $u_\tau = \sqrt{\tau_w/\rho}$ the surface-friction velocity and y_w the wall-normal distance. In terms of eddy viscosity $\nu_t \equiv -\overline{u'v'}/(\mathrm{d}U/\mathrm{d}y)$, we also have

$$\frac{\nu_t}{u_\tau} = \frac{-\overline{u'v'}/u_\tau}{\mathrm{d}U/\mathrm{d}y} = \kappa y_w, \tag{2}$$

while consideration of the mixing length $\ell \equiv (\nu_t/(\mathrm{d}U/\mathrm{d}y))^{1/2}$ gives

$$\ell = \frac{\sqrt{-\overline{u'v'}}}{\mathrm{d}U/\mathrm{d}y} = \kappa y_w. \tag{3}$$

Since $-\overline{u'v'} = \tau(y_w)/\rho = u_\tau^2$ in a constant-stress layer and outside the viscous region, all three expressions are equivalent, and arguing between them probably has limited value. None of the three has a systematic derivation. With pressure gradient, τ/ρ deviates from u_τ^2 and the three proposals conflict, so that at best one of the three will remain effective. This could make such a flow very discriminating, while very accessible to DNS. Ideally, in the near future DNS will be conducted over a fair range of Couette-Poiseuille cases, and new experiments with very fine measurement of the skin friction will be conducted for support and to reach more convincing Reynolds numbers.

Our early results (Johnstone et al. 2010) indicated that the logarithmic-law length scale (1) is much less affected by pressure gradients than the other two options, a finding for which we had (and continue to have) no theoretical justification, nor any strong sense of whether it might be exact, or is only approximate. The demonstration had a preliminary character, due to Reynolds-number limitations and there being only one case. The thickness of the inertial sublayer especially on the adverse-gradient (APG) side was not

large enough to convince all observers. We address, to an extent, this shortcoming in the current computations.

This study can also be viewed as a computational counterpart to the boundary-layer experiments performed by Galbraith & Head (1975) and Galbraith, Sjolander & Head (1977), who long ago were also interested in the relative sensitivity to pressure gradients of the law of the wall (1), eddy viscosity (2) and mixing length (3). Our conclusions again will turn out to be broadly compatible with theirs. We expect boundary-layer DNS to produce the same conclusion, which was already hinted at in Spalart & Watmuff's (1993) adverse-gradient boundary-layer DNS.

Another new element of the present study is results of Reynolds-Averaged Navier-Stokes (RANS) models. These are exercised with and without streamwise vortices, a mode of operation recently proposed with some success by Spalart, Garbaruk & Strelets (2014) for pure Couette flow. Such vortices need to be considered if a rigorous comparison of DNS and RANS results is to be performed, and it is possible their presence also alters the answer to the seemingly simple question regarding the alternative length scales formulated above.

2 Approach and Problem Definition

In order to introduce favorable and adverse pressure gradients and to separate them from the Reynolds number, we consider incompressible Couette-Poiseuille flow, driven by a steady uniform pressure gradient $\mathrm{d}(P/\rho)/\mathrm{d}x$ and in-plane streamwise wall motion, in opposite directions, of speed U_w. This is a two-parameter family of flows. A Reynolds number, based on the wall-velocity difference $\Delta U = 2U_w$ and full channel height $2h$, of $\mathrm{Re} = 80,000$ is prescribed (i.e. twice that of our 2010 study), along with a streamwise pressure gradient $\mathrm{d}(P/\rho)/\mathrm{d}x = -0.0014U_w^2/h$. This leads to non-dimensional pressure gradients $p^+ \equiv \mathrm{d}\tau^+/\mathrm{d}y^+ = [\mathrm{d}(P/\rho)/\mathrm{d}x]\left[\nu/u_\tau^3\right]$ of $p^+ \approx -0.0003$ and $+0.0030$ on the favorable-pressure-gradient (FPG) and adverse-pressure-gradient (APG) sides, respectively. The FPG value of p^+ is the same as in Poiseuille flow with $\mathrm{Re}_\tau = u_\tau h/\nu = 3125$, and therefore quite weak. The simulation uses a parallel version of the Fourier/Chebyshev spectral channel code of Kim, Moin & Moser (1987), from which it differs algorithmically only in that a third-order Runge-Kutta/Crank-Nicolson scheme is used for the time integration (which is formulated in the reference frame moving at the average speed of the two walls).

The simulation was initialized by random disturbances (of amplitude large enough to trigger nonlinear/bypass transition) on an under-resolved grid at lower Reynolds number, and continued until the flow reached a statistically stationary state, after which the Reynolds number was increased to its final value and the flow re-projected onto finer grids multiple times, each advanced to a stationary condition. The results shown below are from the fully resolved state, run sufficiently long (see below) to obtain well-defined statistics averaged in time and in the two homogeneous directions.

Table 1: Run parameters.

Wall	$u_\tau/2U_w$	p^+	Δx^+	Δz^+	y_{10}^+
APG	0.0145	$+0.00285$	5.4	2.7	3.0
FPG	0.0302	-0.00032	11.3	5.6	6.1

At this Reynolds number, a real-space resolution of $n_x \times n_y \times n_z = 1,344 \times 281 \times 1,344$ collocation/quadrature points is required to capture all relevant scales throughout the domain. (The 3/2 rule is applied in x and z for dealiasing.) This grid count, near 0.5×10^9, does not allow multiple simulations to be performed easily. In wall units from the FPG side (i.e. the side with larger u_τ), this corresponds to a time step $\Delta t^+ \approx 0.24$, streamwise and spanwise grid spacing of $\Delta x^+ \approx 11$ and $\Delta z^+ \approx 6$, and wall-normal distance of the 10th grid point $y_{10}^+ \approx 6$. This is more stringent than the 'conventional' guidelines for a spectral method, of $(\Delta x^+, y_{10}^+, \Delta z^+) \leq (20, 10, 7)$, which is preferable when seeking definitive results from DNS (Spalart et al. 2009).

The size of the computational domain is $4\pi h \times 2h \times 2\pi h$, in the streamwise x, wall-normal y and spanwise z directions, respectively. The spanwise domain length L_z is large enough to contain two pairs of large-scale streamwise roll cells, which tend to reach from wall to wall (Figures 2 and 3), typical of those found in pure Couette flow. Johnstone (2014, personal communication) observed similar cells in his lower-Re, larger-domain Couette-Poiseuille DNS, for which $4U_w h/\nu = 40,000$ and $\mathrm{d}(P/\rho)/\mathrm{d}x = -0.00085U_w^2/h$, with $(L_x, L_z) = (16\pi h, 4\pi h)$. It is very likely that much stronger pressure gradients, producing flows closer to the Poiseuille limit than those considered here, are required to prevent the formation of large-scale, domain-filling streamwise rolls cells. The presence of the rolls complicates the interpretation of this flow as a prototype of canonical FPG and APG boundary layers, and thus care must be exercised when using the present results to draw general conclusions regarding turbulence theory and modeling. In particular, the results may depend on the size of the spanwise period, which is arbitrary. This issue will be revisited below.

3 Results

Overall character of the flow

Figure 1 illustrates the asymmetry in the velocity profile introduced by the pressure gradient and moving walls, which still has a strong Couette character

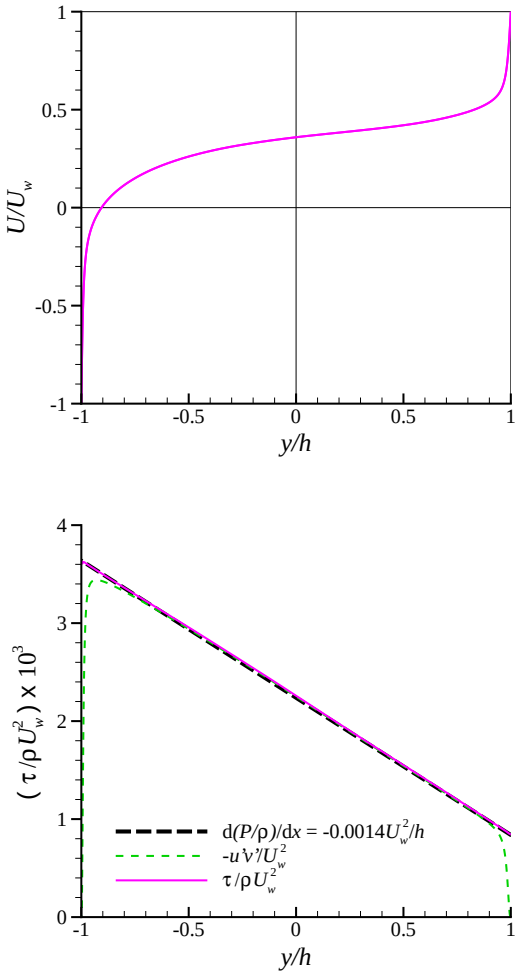

Figure 1: Top, mean velocity; bottom, Reynolds and total shear stress.

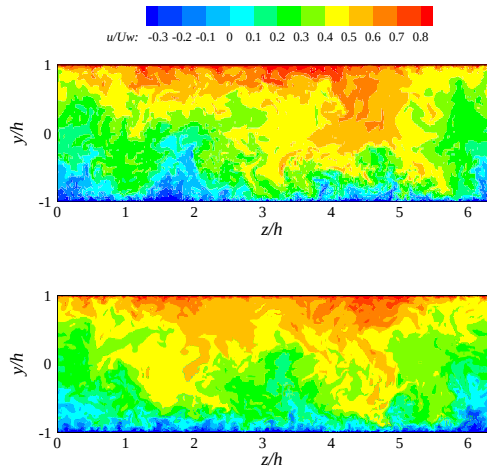

Figure 2: Contours of instantaneous streamwise velocity in vertical-spanwise (y-z) plane from realization at (top) beginning and (bottom) end of averaging period.

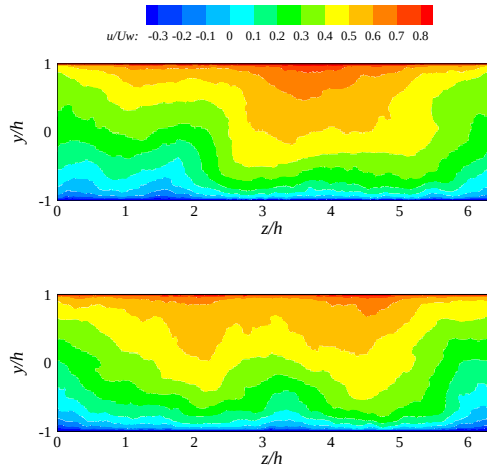

Figure 3: Contours of streamwise-averaged streamwise velocity in vertical-spanwise (y-z) plane from realization at (top) beginning and (bottom) end of averaging period.

with only one sign of $\mathrm{d}U/\mathrm{d}y$ and τ. The effective FPG and APG wall layers are characterized by the negative and positive (with respect to the reference frame attached to each moving wall) wall-normal total shear-stress gradients $\mathrm{d}\tau/\mathrm{d}y_w$ also shown in Figure 1. The level of equilibrium of the time- and (x,z)-plane average, which was gathered over a period of approximately $460h/U_w$, can also be inferred from this figure by comparing the total stress profile to the linear idealization defined by the pressure gradient. This figure also shows that the viscous shear stress is confined to thin regions, compared with h; this widens the region over which pure turbulent behavior can be hoped for.

Although the linear stress profile reflects a mature solution very close to equilibrium, it appears the roll-cell structures may not have reached their final (stationary) configuration at the beginning of the averaging period. This is suggested by the difference between the streamwise-velocity contours in y-z planes at times corresponding to the beginning (top figures) and end (bottom figures) of the averaging, which are shown in figures 2 and 3 (the former showing a single y-z plane, the latter the streamwise-domain average). The difference is consistent with the roll structure 'splitting' laterally from one to two, transitioning from a state in which the roll energy resides primarily in the $(k_x^*, k_z^*) = (k_x L_x/2\pi, k_z L_z/2\pi) = (0, \pm 1)$ mode (where k_x and k_z are the streamwise and spanwise wavenumbers) to one in which $(0, \pm 2)$ dominates. This has been confirmed by examination of the velocity spectra from the channel centerline at the two times in question. The DNS will need to be continued to ascertain whether the roll's final state remains 'locked' into the $(0, \pm 2)$ mode, and to quantify the effect the roll evolution has on the mean profiles shown below.

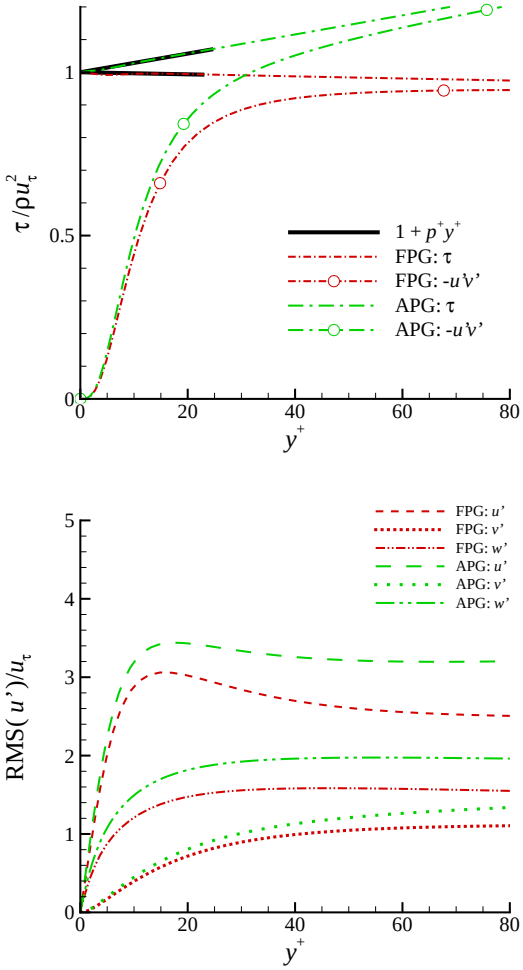

Figure 4: Top, Reynolds- and total-shear stress; bottom, root-mean-squared (RMS) velocity fluctuations, in local wall units.

Figure 4 initiates the comparison of the two wall regions, each with a normalisation based on its own friction velocity. The influence of the pressure gradient on the near-wall variation of the Reynolds stresses is very visible. The thick-solid line near $y^+ = 0$ gives the slope, in wall units, of the total shear stress. The pressure-gradient effect reaches all the way to the wall, especially for the two wall-parallel stresses $\overline{u'u'}$ and $\overline{w'w'}$; in other words, they grossly violate any 'law of the wall,' defined solely in terms of y^+ and u_τ. Note however that even without pressure gradient, when varying Reynolds number the diagonal stresses violate what would be a law of the wall to a similar degree, at least for Reynolds numbers currently accessible to DNS (Spalart 1988, Hoyas & Jiménez 2006).

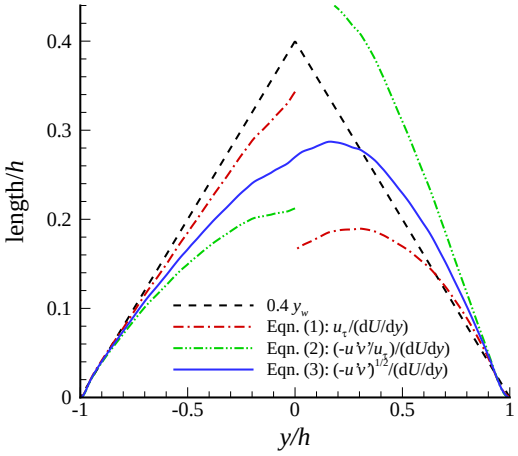

Figure 5: Turbulence length scales.

Comparison between length scales

In Figure 5 we re-visit the question of the pressure-gradient response of the wall-turbulence semi-theories (1), (2) and (3). As in Johnstone et al. (2010), the log-law version of the length scale (1) is found to be significantly less vulnerable to pressure gradient than the other two. This is seen more clearly with the higher Reynolds number, and applies to both walls. Note that the line $l = \kappa y_w$ is not in-between (1) and another curve; in other words, the results do not indicate a mere preference towards (1), they suggest that (3) and especially (2) grossly fail to match reality. This argues against the success of a theory based on a weighted average of the three candidates.

Compared with our first Couette-Poiseuille paper (Johnstone et al. 2010), the higher Reynolds number allows us to refine the conclusions: especially in the region below roughly $y/h = -0.7$, length scale (1) appears to have a smooth and consistent deviation from $\kappa_0 y_w$, where $\kappa_0 = 0.4$. One interpretation could be that this region has a lower value of κ, of the order of 0.375; this value is quite low, even with the current

uncertainty over the exact value of κ. Also note that the same attitude applied near $y = +0.8$ and therefore on the APG side would suggest a higher value than 0.4 for κ. Another interpretation is that the Reynolds number is not sufficient for the result to arrive at the final behavior. However, considering that the Reynolds number has been doubled, it now appears established that the 'resilience' of (1) we noted in our earlier study is not perfect.

The trend seen here is consistent with Galbraith's 1975 experimental findings, which we believe have not been adequately recognized, confirmed, challenged, or adopted as a guide for turbulence modeling. Unfortunately, this line of work remains narrow and isolated.

Detailed behavior of the velocity profile

Having established that the velocity profile is closer to universal behavior than the other candidates, we now study it more closely. The effect of the pressure gradient on the law-of-the-wall scaling of the mean velocity is shown in Figure 6, which includes results from both the present and earlier Couette-Poiseuille DNS, along with the pure-Poiseuille profile from Hoyas & Jiménez (2006), for which $p^+ = -5.0 \times 10^{-4}$ (indicating a weak FPG). The higher Reynolds number of the new simulation is evident in the clearer distinction between the buffer, (nominally) logarithmic, and wake regions for both the FPG and especially the APG sides. The FPG profile agrees well with the reference higher-Reynolds-number profile of Hoyas & Jiménez, while the APG result falls well below the channel benchmark: the viscous sublayers all agree to plotting accuracy, but at larger y^+ the APG profiles dip below the FPG mean; the deviation becomes noticeable near $y^+ = 15$. Note that the grid resolution in wall units is more favorable for this wall, with its lower u_τ, so that a higher level of numerical error near this wall is not suspected. At $y^+ = 30$, the total shear stress is about 8% higher than at the wall, which can already be considered a significant deviation. In other words, if measured by the shear stress the FPG cases are actually clustered very close together, and the APG case is isolated; this makes the behavior of the velocity less surprising.

A more sensitive measure of the velocity profile is presented in Figure 7, in terms of what we refer to as the Kármán measure $\kappa_M = \mathrm{d}(\ln y^+)/\mathrm{d}U^+$. It is equal to the length scale in (1), divided by y^+. Also included are the Hoyas & Jiménez (2006) channel data and results from a series of Ekman-layer DNS over a range of Reynolds numbers (Spalart et al. 2009; Johnstone 2012). The Kármán measure equals the Kármán constant κ in an exactly logarithmic region; the lack of a plateau (expected to begin around $y^+ = 100$, roughly) indicates that such a layer is not present for the flows examined here. This may be blamed on the relatively low Reynolds numbers amenable to DNS, but perhaps not totally, considering that values more than 20 times larger than in the pioneering DNS of the 1980s have

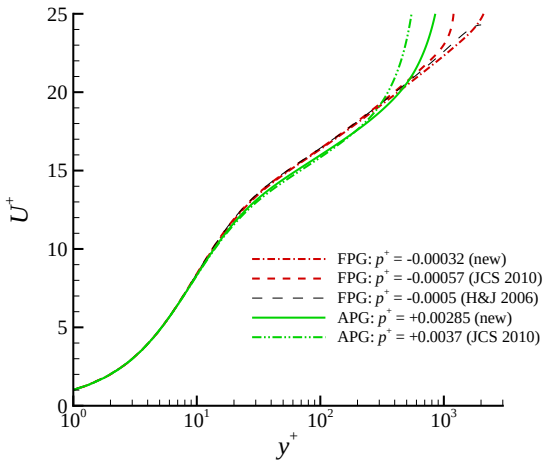

Figure 6: Velocity profiles in wall units. The plane Poiseuille results of Hoyas & Jiménez (2006) are included for comparison ($p^+ = -5.0 \times 10^{-4}$).

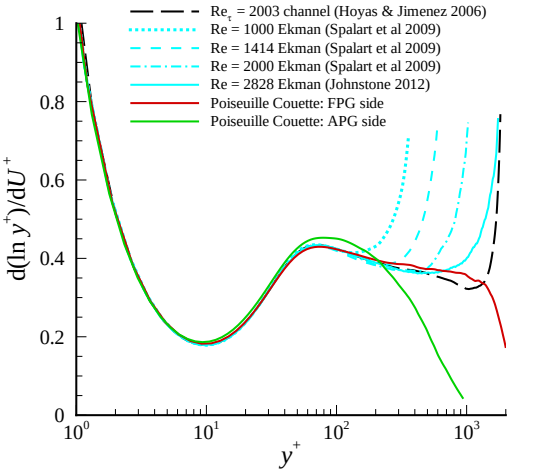

Figure 7: Kármán measure. Included for comparison are DNS results from the plane-Poiseuille flow of Hoyas & Jiménez (2006) and the Ekman-layer profiles of Spalart et al. (2009) and Johnstone (2012).

been reached. If the current thinking among some experimentalists (based on very high Reynolds number pipe-flow measurements) – that a constant-κ region should only be expected for Reynolds numbers large enough that $y^+ = 10^3$ falls well below 0.1δ (where δ is the layer thickness) – then a 'DNS answer' for the value of κ – and confirmation that it is indeed universal – is many years away.

For now, we note that Figures 6 and 7 support the validity of the *general* law of the wall (i.e. that $\mathrm{d}U^+/\mathrm{d}y^+$ depends only on y^+), which is unaffected by system rotation (acting in the Ekman flow) and the sign and magnitude of pressure gradient (in the pure- and Couette-Poiseuille channels), for $0 < y^+ < 35$. Focusing only on the FPG results, a further case can be made that the range of established universality extends to $y^+ \approx 400$ or so, since the rotating-boundary-layer and channel results agree here. The trend versus Reynolds number is very encouraging. Although some questions remain open, this finding tends to contradict claims made by some that even the high-Reynolds-number limit of κ would be flow-type dependent, that is, different for example in channels, pipes and various versions of boundary layers. The behavior in APG is a little dissonant, but we pointed out that its pressure gradient in wall units is still fairly strong.

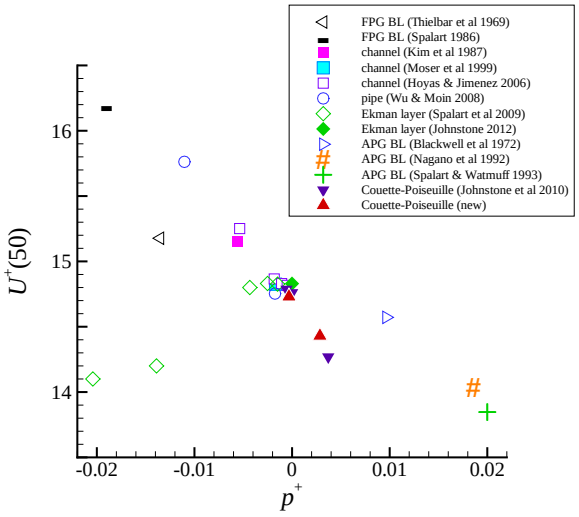

Figure 8: Values of U^+ at $y^+ = 50$ for various pressure gradients, from experiment and simulation. New results are shown by solid red upward triangles.

We return to the pronounced downward shift with increasing p^+ seen for $y^+ > 15$ in Figure 6. Figure 8 (essentially the same as Figure 6 in Johnstone et al.) documents the variation of $U^+(50)$, the velocity at $y^+ = 50$, for a range of pressure gradients. This includes a wide group of earlier DNS and experiments, some with much stronger values of p^+ than the present ones, in both directions. The new results are in line with the old ones. Both our old and new APG results are somewhat below the general trend. The results are compatible with the conjecture that $U^+(50)$ primarily depends on p^+, as opposed to other parameters such as Reynolds number. The general conjecture would be that the velocity profiles follow a law of the type $U^+ = f(y^+, p^+)$, with the flow Reynolds number and other measures of the outer flow having a much weaker effect than p^+ does, over a useful range of y/δ where δ is a measure of the outer-layer thickness. Such a finding could be used to construct a pressure-gradient-dependent wall function for U^+ in non-separated boundary layers. However, there are many issues with this, such as the difference between p^+ and $\mathrm{d}\tau^+/\mathrm{d}y^+$ in flows other than channels (Johnstone et al. 2010). Finally, recall that mixing-length reasoning would predict a positive slope in this figure (Spalart & Watmuff 1993), thus repeating the egregious failure of that approximation seen in Figure 5.

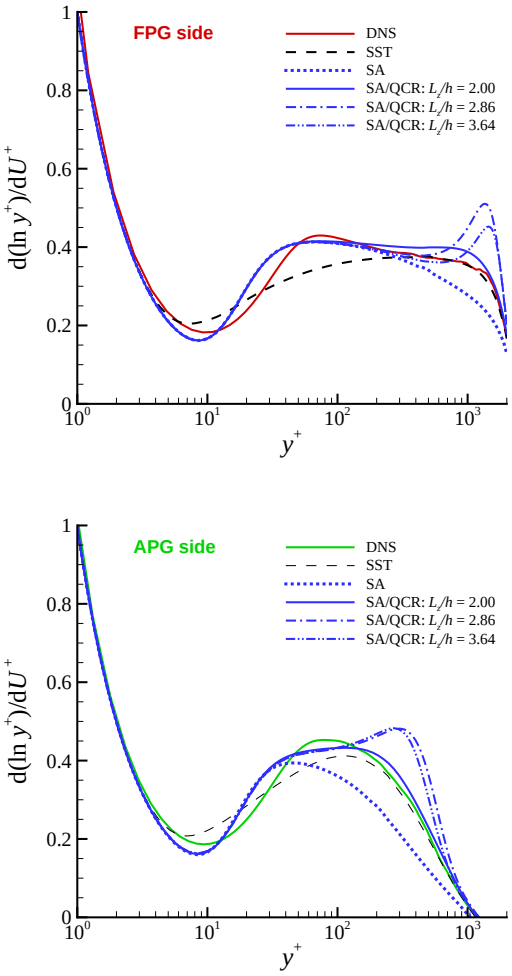

Figure 9: Kármán measure implied by SST and SA models.

Results of turbulence models

We conclude by examining the ability of two widely-used RANS models to reproduce the DNS results, with attention given to possible roll-cell effects.

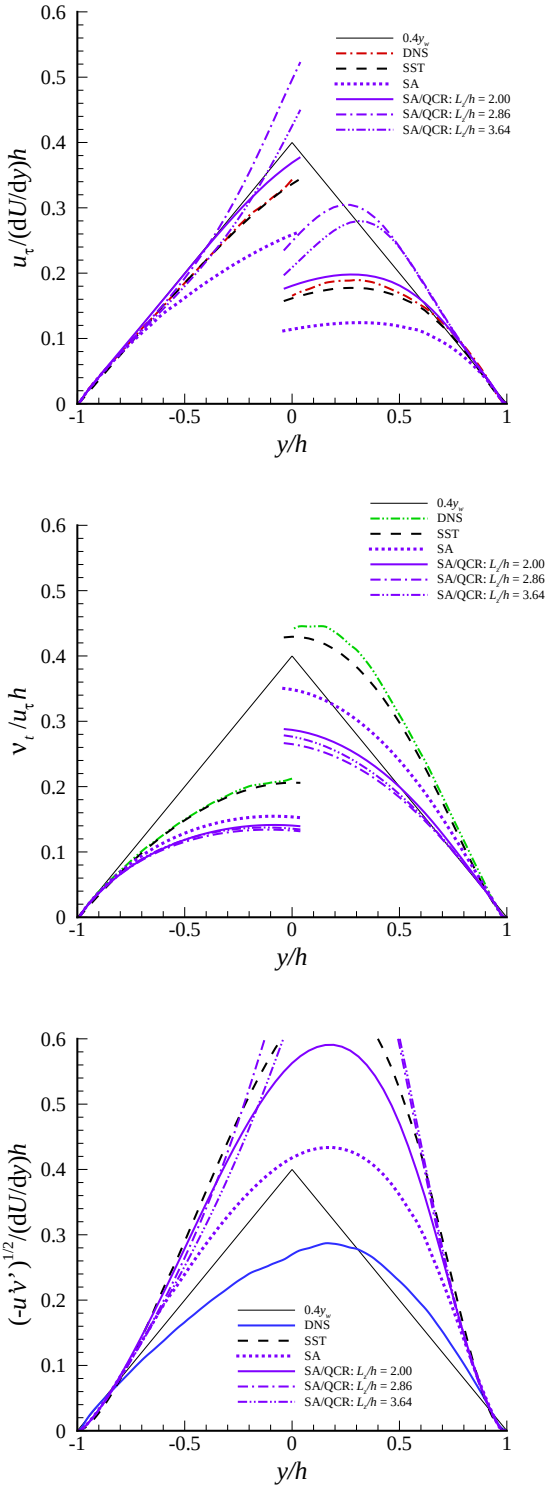

Figure 10: Turbulence length scales implied by SST and SA models.

The models are Menter's (1994) SST and the Spalart-Allmaras (1994) (SA) models, the latter with and without the quadratic-constitutive-relation (QCR) option (Spalart 2000). The SA/QCR model is exercised in the spanwise-periodic mode introduced, in a study of pure Couette flow by Spalart et al. (2014), with various values for the period L_z, which controls the 'roll cells.' Briefly, the approach is to obtain RANS solutions that are steady and independent of x, but have a z dependence and three velocity components: (U, V, W) are functions of (y, z). Spalart et al. (2014) found that eddy-viscosity models combined with a simple QCR (and only these models, so far) sustain roll cells that resemble those known in Couette-flow experiments and DNS (evoking Figure 3), and account for sometimes half of the momentum transfer in the core region of the flow. It was also found that this transfer depends quite strongly on the rolls' spanwise spacing, which is arbitrary within a range; that is, the equations accept the rolls only over a band of wavelengths. Note that the $(k_x^*, k_z^*) = (0, \pm 2)$ mode associated with the DNS rolls in Figure 3(bottom) implies their lateral spacing is $\lambda_z = L_z/2 = \pi h$, such that an SA/QCR run with $L_z/h = \pi$ corresponds to the most mature DNS spacing.

The Kármán-measure profiles are shown in Figure 9. The SST model is not very accurate in the buffer layer; this is a known issue, ultimately tied to the non-use of a viscous damping function similar to f_{v1} in the SA model. Farther from the wall, SST is in noticeably better agreement with DNS than SA, unless SA/QCR is used with the most favorable value of L_z/h, namely 2 (a value which gives the best results for both walls, but is not very close to the current DNS value, namely π). This confirms that the roll cells have a major influence on the RANS results, not only in Couette flow but also in the present blend with Poiseuille flow. Runs with SST-QCR and roll cells will also be instructive, although the use of the model without roll cells is certainly appropriate.

In Figure 10, we examine the three length scales as produced by the turbulence models. It confirms Figure 9 in terms of ranking the models for accuracy. The figure also gives a commentary on the nature of transport-equation turbulence models, as opposed to algebraic models. A mixing-length algebraic model would agree precisely with equation (3), for instance, up to some distance from the wall of order h. This does not happen with either of the present models. These models were constrained to agree with (1), (2) and (3) in a constant-stress layer, and it could have been that they fortuitously agree with one of the three in general. Instead, they agree with (1) better than (2) or (3); this is a favorable trend, since this is also what DNS does, but this is not by design and simple behavior is not to be expected. In the SA model, the behavior could become 'by design' if the f_w function were adjusted to match new results.

4 Summary and Future Work

A new Couette-Poiseuille DNS is used to explore the universality and robustness of conflicting versions of near-wall similarity. The impact of pressure gradient on the log-law relationship for the mean velocity is found to be significantly weaker than it is on eddy-viscosity and mixing-length alternatives. Compared to our previous findings, the present conclusions are less clouded by low-Reynolds-number effects, and are thus more compelling. On the other hand, the effect of the large-scale streamwise roll cells/vortices suspected in the DNS is not yet fully resolved, and we must not over-estimate the authority of RANS results for such phenomena. The reality is that Couette-Poiseuille DNS is far from immune to the problem of domain size that affects Couette flow.

We again take note of an encouraging trend among many datasets for a possible pressure-gradient-based correction of the log law in Figure 8, but recognize that a much larger body of evidence is needed before serious proposals are made.

Further DNS (now underway) is needed to complete the study. We aim to quantify the evolution of the roll structure, and its effect on both the dynamics of the flow (in terms of momentum transport) and the implications for turbulence theory and RANS modeling. It is remotely possible that the ranking of the 'winners' in the length-scale 'contest' (Figure 5) will be re-ordered once this is done. This will involve examining time- as well as streamwise-averaged fields, to ascertain whether a cell remains at a fixed spanwise location, meanders in time and/or streamwise direction, or even has a finite life. A plausible separation of the Reynolds stresses into 'roll-cell' and 'small-scale' contributions would be used after studying the two-dimensional spectra in the x-z plane. Statistics gathered from fields that have had the energy of the modes corresponding to the cells removed would be used to recompute the length-scale profiles examined above.

In the longer term, the pressure gradient and the wall-velocity difference will not have to be in the same direction, so that skewed wall-bounded flows can be simulated by the same method, and compared with the Ekman layer.

Acknowledgments

This project was sponsored by the Revolutionary Computational Aerosciences project under NASA's Fundamental Aerodynamics program. The computations were performed on the NASA Advanced Supercomputing (NAS) Division and the UK/EPSRC HECToR system, via the UK Turbulence Consortium (EPSRC Grant EP/G069581/1). We are grateful to Dr. Roderick Johnstone for his many contributions to this study.

References

Blackwell, B.F, Kays, W.M. & Moffat, R.J. (1972) *The Turbulent Boundary Layer on a Porous Plate: An Experimental Study of the Heat Transfer Behavior with Adverse Pressure Gradients.* HMT-16, Thermosciences Division, Mechanical Engineering Department, Stanford University.

Galbraith, R.A.McD. & Head, M.R. (1975) Eddy viscosity and mixing length from measured boundary layer developments, *Aeronaut. Quart.*, Vol. 26, pp. 133-154.

Galbraith, R.A.McD., Sjolander, S. & Head, M.R. (1977) Mixing length in the wall region of turbulent boundary layers, *Aeronaut. Quart.*, Vol. 27, pp. 229-242.

Hoyas, S. & Jiménez, J. (2006) Scaling of the velocity fluctuations in turbulent channels up to $Re_\tau = 2003$, *Phys. Fluids*, Vol. 18, 011702.

Johnstone, R., Coleman, G.N. & Spalart, P.R. (2010) The resilience of the logarithmic law to pressure gradients: evidence from direct numerical simulation, *J. Fluid Mech.*, Vol. 643, pp. 163-175.

Johnstone, R. (2012) Personal communication.

Kim, J., Moin, P. & Moser, R.D. (1987) Turbulence statistics in a fully developed channel flow at low Reynolds number, *J. Fluid Mech.*, Vol. 177, pp. 133-166.

Menter, F.R. (1994) Two-equation eddy-viscosity turbulence models for engineering applications, *AIAA J.*, Vol. 32, pp. 1598-1605.

Nagano, Y., Tagawa, M. & Tsuji, T. (1992) Effects of adverse pressure gradient on mean flows and turbulence statistics in a boundary layer, In *Turbulent Shear Flows 8*, (ed. F. Durst, B.E. Launder & R. Friedrich), Springer.

Spalart, P. R. (1986) Numerical study of sink-flow boundary layers, *J. Fluid Mech.*, Vol. 172, pp. 307-328.

Spalart, P. R. (1988) Direct simulation of a turbulent boundary layer up to R_θ = 1410, *J. Fluid Mech.*, Vol. 187, pp. 61-98.

Spalart, P.R. & Watmuff J. H. (1993) Experimental and numerical study of a turbulent boundary layer with pressure gradients, *J. Fluid Mech.*, Vol. 249, pp. 337-371.

Spalart, P.R. (2000) Strategies for turbulence modelling and simulations, *Int. J. Heat Fluid Flow*, Vol. 21, 252-263.

Spalart, P.R. & Allmaras, S. (1994) A one-equation turbulence model for aerodynamics flows, *Rech. Aèrospat.*, Vol. 1, 5-21.

Spalart, P.R., Coleman, G.N. & Johnstone, R. (2009) Retraction: Direct numerical simulation of the Ekman layer: A step in Reynolds number, and cautious support for a log law with a shifted origin, *Phys. Fluids*, Vol. 21, 109901.

Spalart, P.R., Garbaruk, A. & Strelets, M. (2014) RANS solutions in Couette flow with streamwise vortices, to appear, *Int. J. Heat Fluid Flow*.

Thielbar, W.H, Kays, W.M. & Moffat, R.J. (1969) *The Turbulent Boundary Layer: Experimental Heat Transfer with Blowing, Suction and Favorable Pressure Gradient.* HMT-5, Thermosciences Division, Mechanical Engineering Department, Stanford University.

Wu, X. & Moin, P. (2008) A direct numerical simulation study on the mean velocity characteristics in turbulent pipe flow, *J. Fluid Mech.*, Vol. 608, pp. 81-112.